Supplementary Information

Universal kinetic description for the thermal dehydration of sodium carbonate monohydrate powder across different temperatures and water vapor pressures

Shunsuke Fukunaga, Yuto Zushi, Mito Hotta, and Nobuyoshi Koga*
Department of Science Education, Graduate School of Humanities and Social Sciences, Hiroshima University, 1-1-1 Kagamiyama, Higashi-Hiroshima 739-8524, Japan

Contents

* Corresponding author. E-mail: nkoga@hiroshima-u.ac.jp

S1. Instrumental setup

(1) Calibration of TG–DTA instruments

Three TG–DTA instruments were employed for tracking of the thermal dehydration of SC-MH, as listed in Table S1. Prior to data collection, all instruments were calibrated with regard to the measured sample temperature and mass change. The sample temperature was calibrated according to the standard procedures, whereby the onset temperature of pure metal melting was measured by DTA signal. The pure metals of In, Sn, Pb, Zn, Al, and Ag (>99.99%, Nilaco) were used as the temperature standard. The measurements were conducted under specific conditions listed in Table S1. The mass change was calibrated using a standard weight of 5 mg by addition/removal to/from the sample holder in the open condition. Furthermore, the three-step mass loss process of the thermal decomposition of $CaC_2O_4 \cdot H_2O$ (~5.00 mg, >99.9985%, Alfa Aesar) was recorded under the specific conditions listed in Table S1 for confirming the appropriateness of the recorded mass change values for the respective thermal decomposition steps.

Table S1. TG–DTA instruments and these calibration conditions

TG–DTA instrument				Measurement conditions for calibration	
Type	Manufacturer	Configuration	Thermocouple	β/K min^{-1}	Atmosphere
DTG-60	Shimadzu	Top loading	K	5	Flowing dry N_2 (q_v = 100 cm^3 min^{-1})
TG-8121	Rigaku	Horizontal	R	5	Flowing dry N_2 (q_v = 300 cm^3 min^{-1})
TG-8120	Rigaku	Horizontal	R	5	Flowing wet N_2 ($p(H_2O)$ = 3.7 kPa, q_v = 400 cm^3 min^{-1})

(2) TG–DTA measurements in a stream of wet N_2

Figure S1 shows the instrumental setup for TG–DTA measurements in a stream of wet N_2 with controlled $p(H_2O)_{ATM}$ values, which is composed of the TG–DTA instrument (TG-8120, Thermoplus 2, Rigaku), the humidity controller (HUM-1, Rigaku), the temperature-controlled water circulator (RT4, Vivo), the temperature-controlled transfer tube, and the hygrometer (HF5 sensor with HF535 converter, rotronic). The electric furnace, the reaction tube, and its anterior chamber were preheated to a temperature above 15 K from the dew point of the wet N_2 to be flowed during the TG–DTA measurements by circulating temperature-controlled water using the circulator. In particular, the temperature of the anterior chamber was controlled to maintain a constant temperature during the measurement. Similarly, the transfer tube was electrically heated at that temperature. The temperature of the saturation bath in the humidity controller was controlled to be a temperature, and N_2 gas was bubbled to produce a wet N_2 gas saturated with water vapor at the temperature of the saturation bath. The wet N_2 gas was mixed with dry N_2 gas and transferred to the anterior chamber at a q_v of approximately 400 cm^3 min^{-1} through the temperature-controlled transfer tube. The hygrometer was used to monitor the temperature and relative humidity (RH%) of the wet N_2 in the anterior chamber. The RH% value of flowing wet N_2 gas was regulated for achieving the preset RH% by controlling the mixing ratio of wet and dry N_2 gas using the mass flow meter in the humidity controller via PID control, with feedback from the hygrometer. In addition, dry N_2 gas was introduced from the rear of the balance system in the TG–DTA system at a q_v of 50 cm^3 min^{-1} to prevent wet N_2 from entering into the balance system. The wet N_2 and dry N_2 were exhausted through the vent located at the contact between the reaction tube and the balance system.

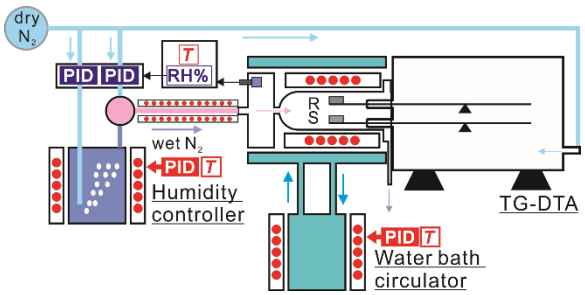

Figure S1. Schematic illustration of the humidity-controlled TG system. Adapted from Yamamoto et al. (DOI: 10.1021/acs.jpcc.0c02739), with permission. Copyright 2020 American Chemical Society.

Prior to conducting TG–DTA measurements, the preset RH% value of the wet N_2 flowing in the reaction tube was established. Subsequently, the weighed sample was placed within the TG–DTA instrument, and the measurements were conducted in accordance with the isothermal and linear nonisothermal heating programs described in the main text. For measurements conducted at $p(H_2O)$ values exceeding 6 kPa, the experiment commenced with a lower RH% value below the preset RH% value during the thermal dehydration process to prevent the hydration reaction of SC-MH. The sample was initially heated to 338 K and maintained at this temperature for 30 min. As the isothermal holding section commenced, the RH% value of the wet N_2 was increased to the preset RH% value. Once the measurement system had been stabilized during the isothermal holding section, the TG–DTA measurements were initiated.

S2. Sample characterization

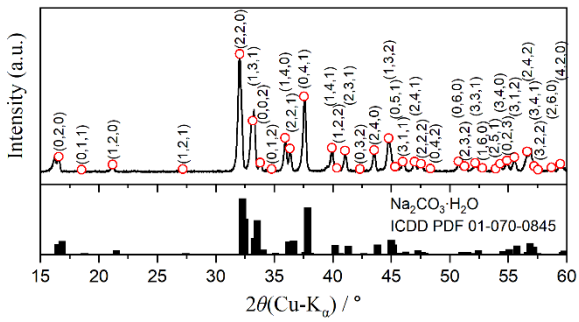

Figure S2. XRD pattern of $Na_2CO_3{\cdot}10H_2O$ efflorescence product (SC-MH).

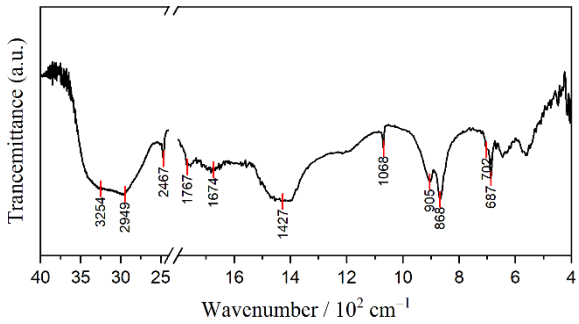

Figure S3. FTIR spectrum of $Na_2CO_3{\cdot}10H_2O$ efflorescence product (SC-MH).

Table S2. Assignment of IR absorption peaks observed for $Na_2CO_3{\cdot}10H_2O$ efflorescence product (SC-MH)[44]

Wavenumber / cm^{-1}	Assignment
3254	O–H stretching
2949	$2\nu_4$ (CO_3^{2-})
2467	$\nu_1 + \nu_4$ (CO_3^{2-})
1767	$\nu_1 + \nu_3$ (CO_3^{2-})
1674	bending mode of O–H
1427	ν_4 (CO_3^{2-})
1068	ν_1 (CO_3^{2-})
868	ν_2 (CO_3^{2-})
702 and 687	ν_3 (CO_3^{2-})

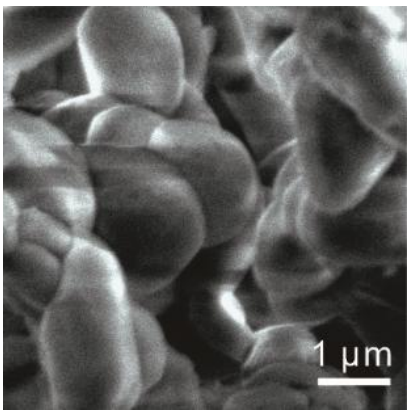

Figure S4. SEM image of $Na_2CO_3{\cdot}10H_2O$ efflorescence product (SC-MH).

S3. Thermal behavior in a stream of dry N_2

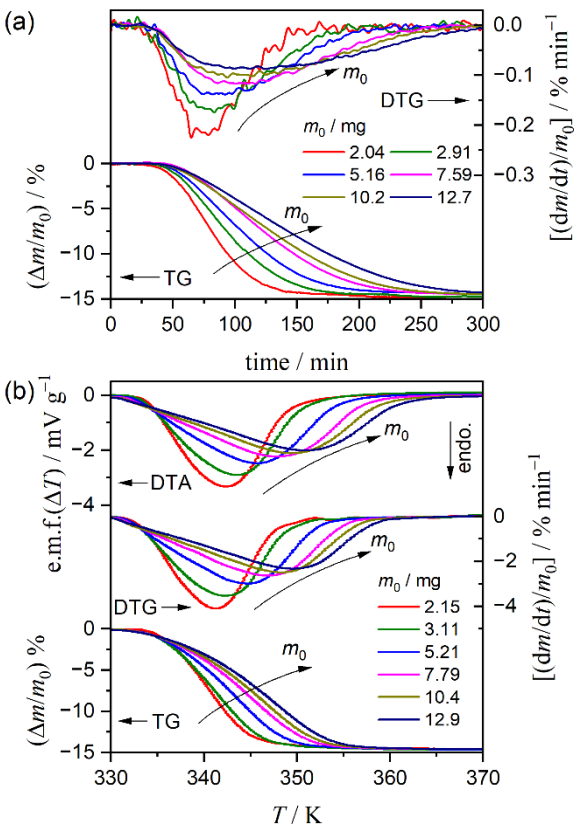

Figure S5. Influence of m_0 on the TG–DTG–DTA curves for the thermal dehydration of SC-MH to form SC-AH in a stream of dry N_2 (q_v = 100 cm^3 min^{-1}): (a) under isothermal conditions at 315 K and (b) under linear nonisothermal conditions at a β of 3 K min^{-1}.

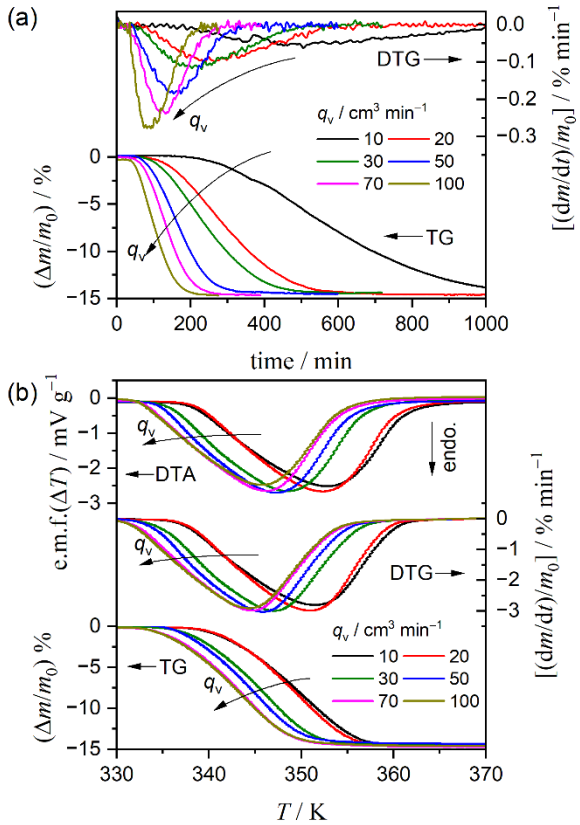

Figure S6. Influence of dry N_2 flow rate (q_v) on the TG–DTG–DTA curves for the thermal dehydration of SC-MH to form SC-AH: (a) under isothermal conditions at 315 K (m_0 = 5.02 ± 0.03 mg) and (b) under linear nonisothermal conditions at a β of 3 K min^{-1} (m_0 = 5.01 ± 0.02 mg).

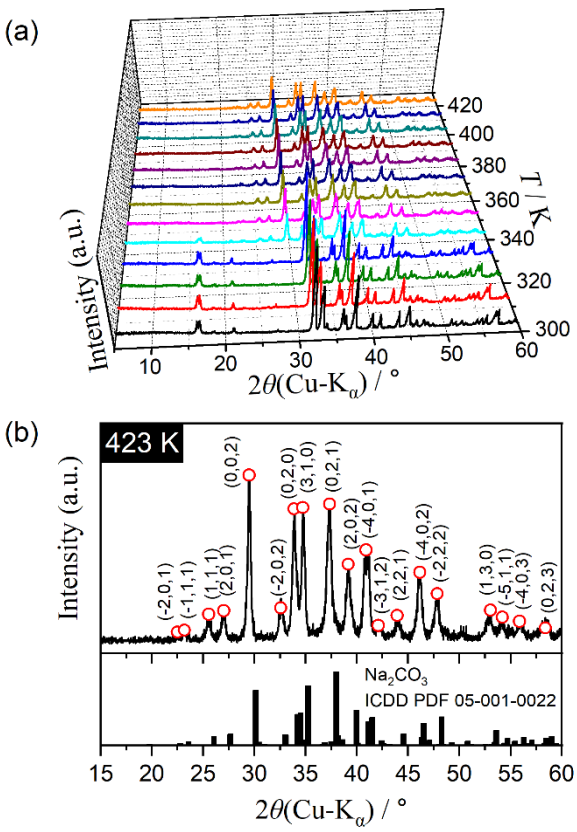

Figure S7. Changes in the XRD pattern of the SC-MH sample during heating under stepwise isothermal conditions in a stream of dry N_2: (a) overview and (b) identification of the XRD pattern at 423 K.

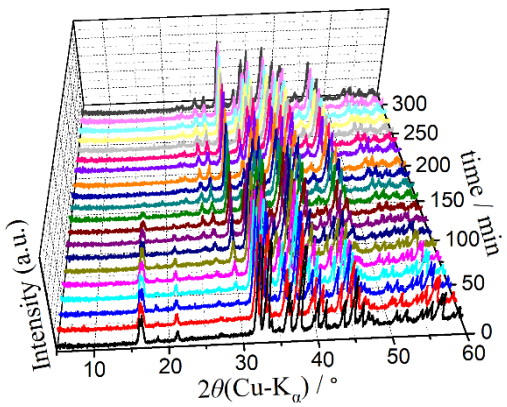

Figure S8. Changes in the XRD pattern of the SC-MH sample during heating under isothermal conditions at 333 K in a stream of dry N_2.

S4. Conventional kinetic analysis

Table S3. Apparent kinetic parameters for the IP process under individual atmospheric conditions, determined by the conventional kinetic analysis ignoring the effect of $p(H_2O)$

$p(H_2O)_{ATM}$ / kPa	$E_{a,IP}$ / kJ mol^{-1}	ln(A_{IP} / s^{-1})	$-\gamma$ [a]
dry N_2 (< 0.2)	186.7 ± 12.4	63.8 ± 4.7	0.9830
0.4	254.3 ± 10.2	86.6 ± 3.8	0.9960
3.6	317.8 ± 20.7	104.4 ± 7.3	0.9916
8.9	481.3 ± 56.1	156.0 ± 19.0	0.9739

[a] Correlation coefficient of the linear regression analysis for the Arrhenius plot.

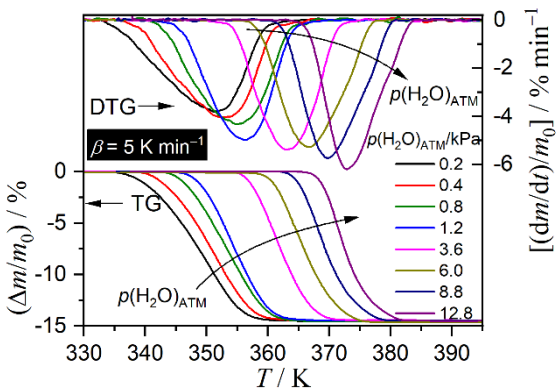

Figure S9. TG–DTG curves for the thermal dehydration of SC-MH (m_0 = 5.01 ± 0.05 mg) under linear nonisothermal conditions at a β of 5 K min^{-1} in a stream of wet N_2 with different $p(H_2O)_{ATM}$ values.

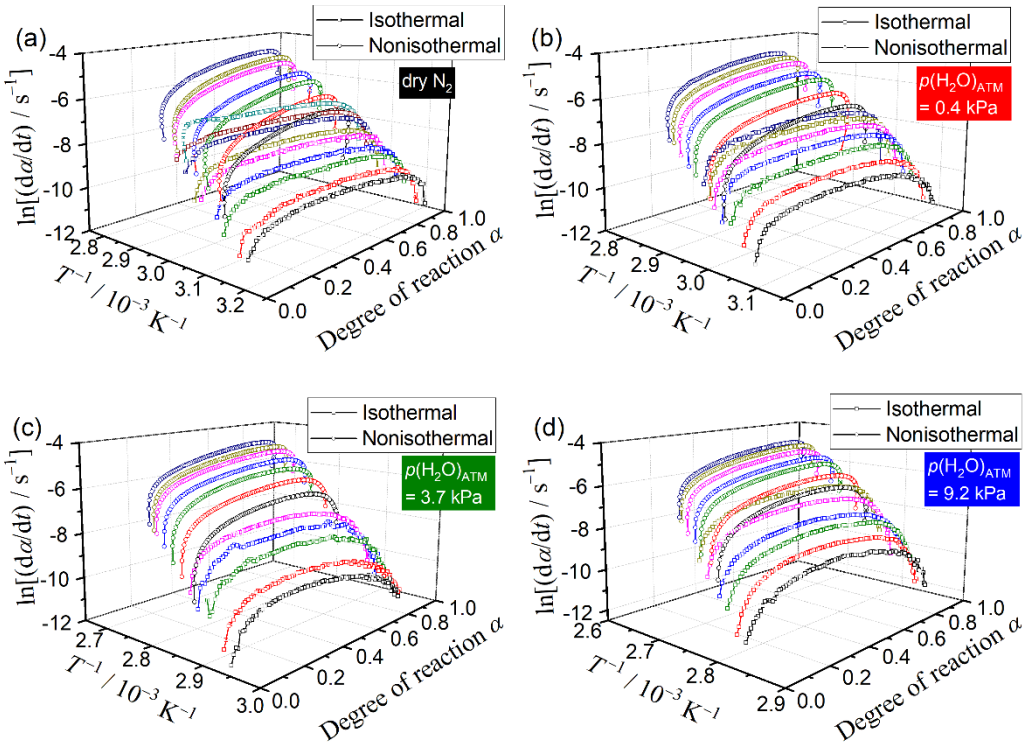

Figure S10. Kinetic data, represented in the 3D kinetic coordinate of T^{-1}, α, and ln(dα/dt), for the thermal dehydration of SC-MH in a stream of dry or wet N_2 with different $p(H_2O)_{ATM}$ values: (a) dry N_2 ($p(H_2O)_{ATM}$ < 0.2 kPa), (b) wet N_2 ($p(H_2O)_{ATM}$ = 0.4 kPa), (c) wet N_2 ($p(H_2O)_{ATM}$ = 3.7 kPa), and (d) wet N_2 ($p(H_2O)_{ATM}$ = 9.2 kPa).

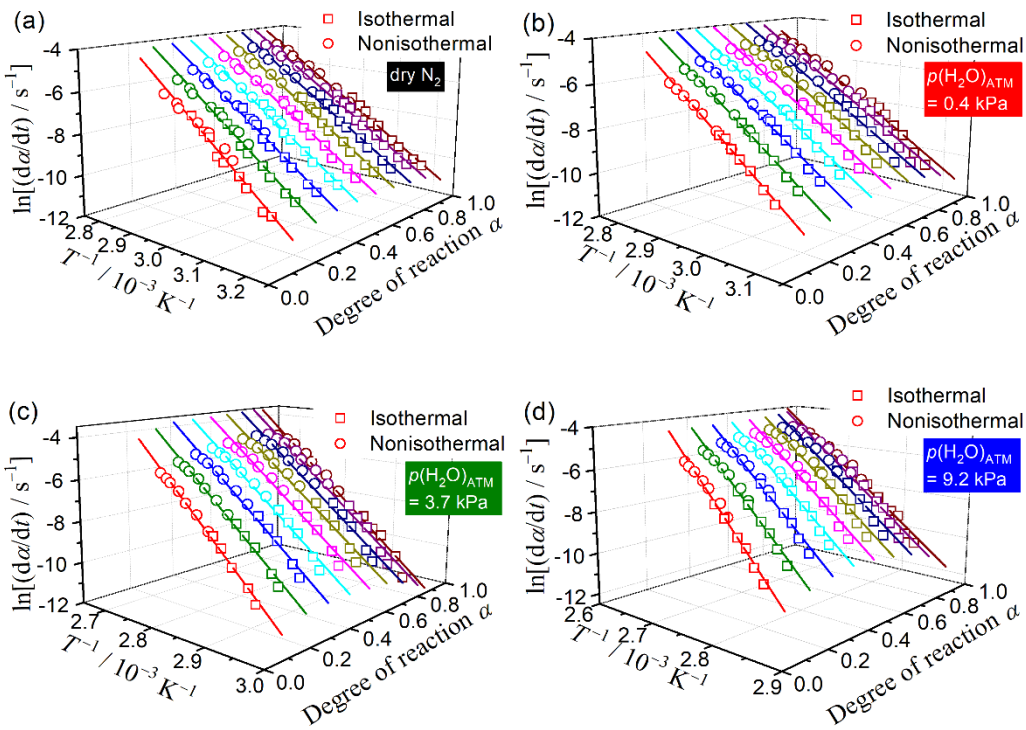

Figure S11. Friedman plots at various α values from 0.10 to 0.90 in steps of 0.10 for the thermal dehydration of SC-MH in a stream of dry or wet N_2 with different $p(H_2O)_{ATM}$ values: (a) dry N_2 ($p(H_2O)_{ATM}$ < 0.2 kPa), (b) wet N_2 ($p(H_2O)_{ATM}$ = 0.4 kPa), (c) wet N_2 ($p(H_2O)_{ATM}$ = 3.7 kPa), and (d) wet N_2 ($p(H_2O)_{ATM}$ = 9.2 kPa).

Table S4. Results of the conventional kinetic analysis of the thermal dehydration of SC-MH under individual atmospheric conditions in a stream of dry or wet N_2 with different $p(H_2O)_{ATM}$ values

$p(H_2O)_{ATM}$/kPa	E_a / kJ mol^{-1}, [a]	$d\alpha/d\theta = Af(\alpha)$					
		$f(\alpha)$	A / s^{-1}	m	n	p	R^2, [f]
dry N_2	115.5 ± 6.8	SB(m, n, p) [b]	$(2.75 \pm 0.07) \times 10^{15}$	0.21 ± 0.29	0.59 ± 0.11	0.01 ± 0.28	0.9876
		R(n) [c]	$(1.16 \pm 0.01) \times 10^{15}$	-----	1.82 ± 0.03	-----	0.9852
0.4	132.8 ± 8.2	SB(m, n, p) [b]	$(6.16 \pm 0.14) \times 10^{17}$	0.15 ± 0.26	0.74 ± 0.10	0.21 ± 0.25	0.992
		R(n) [d]	$(2.20 \pm 0.03) \times 10^{17}$	-----	2.05 ± 0.05	-----	0.9849
3.7	197.9 ± 8.8	SB(m, n, p) [b]	$(7.77 \pm 0.16) \times 10^{26}$	0.64 ± 0.29	1.04 ± 0.11	−0.12 ± 0.28	0.9980
		R(n) [e]	$(1.21 \pm 0.05) \times 10^{26}$	-----	3.39 ± 0.18	-----	0.9839
9.2	246.9 ± 25.6	SB(m, n, p) [b]	$(2.02 \pm 0.02) \times 10^{33}$	−1.25 ± 0.13	1.82 ± 0.06	1.81 ± 0.13	0.9996
		R(n) [e]	$(3.75 \pm 0.14) \times 10^{32}$	-----	2.93 ± 0.15	-----	0.9788

[a] Averaged range: $0.10 \leq \alpha \leq 0.90$.
[b] Fitted range: $0.01 \leq \alpha \leq 0.99$.
[c] Fitted range: $0.40 \leq \alpha \leq 0.95$.
[d] Fitted range: $0.50 \leq \alpha \leq 0.95$.
[e] Fitted range: $0.40 \leq \alpha \leq 0.80$.
[f] Determination coefficient of the nonlinear least-squares analysis.

S5. Formulation of accommodation function

In order to formulate the accommodation function (AF) of describing the dependence of the reaction rate on $p(H_2O)$, the classical surface nucleation and interfacial reaction theories were adopted. It was assumed that the IP and the initial stage of the mass loss process of the thermal dehydration would obey the surface nucleation theory. Moreover, the established stage of the mass loss process can be described by the interfacial reaction theory. Both the surface nucleation and the interfacial reaction can be described by a series of consecutive or concurrent elementary steps. The surface reaction process can be divided into three elementary steps.

(1S) Desorption of water molecules from the surface
(2S) Creation of water vacancy in the surface
(3S) Consumption of vacancy and formation of the product phase of SC-AH on the surface

In addition, five elementary steps can be assumed for the interfacial reaction.

(1I) Desorption of water molecules from the external interface
(2I) Adsorption of water molecules on the external interface
(3I) Diffusion of interstitial water molecule from the internal to the external interface
(4I) Creation of interstitial water molecule and vacancy at the internal interface
(5I) Consumption of vacancy and formation of the product phase of SC-AH at the internal interface

These elementary steps of the surface nucleation and interfacial reaction are expressed using Kröger's notation in Tables S5 and S6, respectively. The equilibrium constant of each elementary step, K_i, is also provided in these tables. When one elementary step is selected as the rate-determining step and the other elementary steps are assumed to be in equilibrium, the kinetic equation controlled by each elementary step is derived as listed in the last column of these tables. Notably, all kinetic equations are composed of $p(H_2O)$ and $P_{eq}(T)$. Thus, the AF is expressed as a function of $p(H_2O)$ and $P_{eq}(T)$, that is, $h(p(H_2O), P_{eq}(T))$. The changes in $P_{eq}(T)$ of the thermal dehydration of SC-MH with temperature are illustrated in Figure S12. The thermal dehydration of SC-MH occurs at higher temperatures than the equilibrium temperature at a fixed $p(H_2O)$ and at lower $p(H_2O)$ values than the equilibrium pressure at a fixed temperature. With several approximations, all these equations can be expressed by an analytical form with the exponents (a, b) as shown in eq. (10) in the main article.

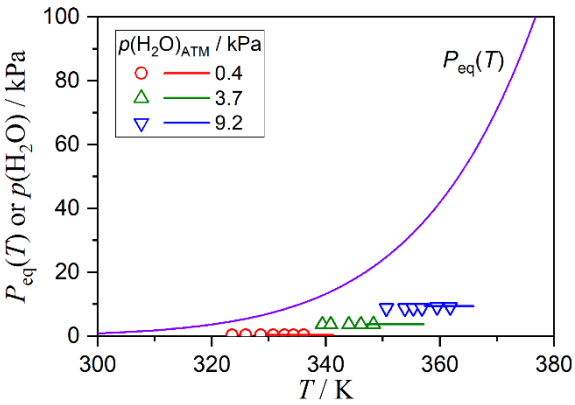

Figure S12. $P_{eq}(T)$ values at various temperatures for the thermal dehydration of SC-MH and the range of (T, $p(H_2O)_{ATM}$) values of the experimental kinetic curves obtained in this study.

S6. Extended kinetic analysis considering the effect of water vapor

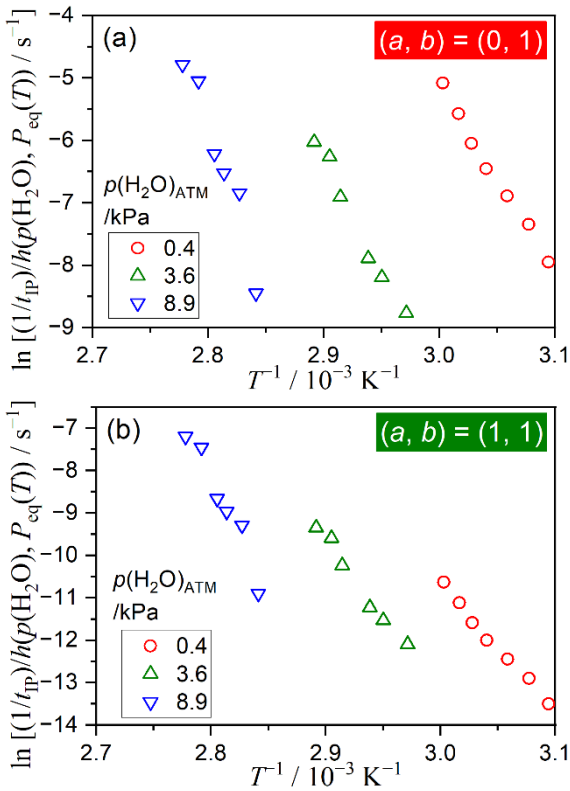

Figure S13. Extended Arrhenius plots for the IP process of the thermal dehydration of SC-MH in a stream of wet N_2 with different $p(H_2O)_{ATM}$ values, examined according to eq. (11) with (a) (a, b) = (0, 1) and (b) (a, b) = (1, 1).

Table S5. Elementary steps assumed for the surface nucleation process of the thermal dehydration of SC-MH, the respective equilibrium constants, and the kinetic equations derived based on the rate-determining step and steady-state approximations

Elementary step	Reaction	Equilibrium constant, K_i	Overall rate v_i for the process controlled by the elementary step i
(1S)	$\mathrm{H_2O-(s)} \rightleftarrows \mathrm{H_2O(g)+(s)}$	$K_1 = \frac{[(\mathrm{s})]\left(p(\mathrm{H_2O})\right)}{[\mathrm{H_2O{-}(s)}]}$	$v_1 = k_1 \frac{K_3^{1/n} K_2}{1 + K_3^{1/n} K_2}\left(1 - \frac{p(\mathrm{H_2O})}{P_{\mathrm{eq}}(T)}\right)$
(2S)	$\mathrm{H_2O_{H_2O}+(s)} \rightleftarrows \mathrm{H_2O{-}(s)+V_{H_2O}}$	$K_2 = \frac{[\mathrm{H_2O{-}(s)}]\left[\mathrm{V_{H_2O}}\right]}{[(\mathrm{s})]}$	$v_2 = k_2 \frac{K_1}{K_1 + p(\mathrm{H_2O})}\left(1 - \frac{p(\mathrm{H_2O})}{P_{\mathrm{eq}}(T)}\right)$
(3S)	$n\left[\mathrm{2Na_{Na}+CO_{3,CO_3}+V_{H_2O}}\right]_h \rightleftarrows n\left[\mathrm{2Na_{Na}+CO_{3,CO_3}}\right]_a$	$K_3 = \frac{1}{\left[\mathrm{V_{H_2O}}\right]^n}$	$v_3 = k_3 \left(\frac{K_1 K_2}{p(\mathrm{H_2O})}\right)^n \left(1 - \frac{p(\mathrm{H_2O})^n}{P_{\mathrm{eq}}(T)^n}\right)$

Table S6. Elementary steps assumed for the interfacial reaction process of the thermal dehydration of SC-MH, the respective equilibrium constants, and the kinetic equations derived based on the rate-determining step and steady-state approximations

Elementary step	Reaction	Equilibrium constant, K_i	Overall rate v_i for the process controlled by the elementary step i
(1I)	$\mathrm{H_2O-(s)} \rightleftarrows \mathrm{H_2O(g)+(s)}$	$K_1 = \frac{[(\mathrm{s})]\left(p(\mathrm{H_2O})\right)}{[\mathrm{H_2O{-}(s)}]}$	$v_1 = k_1 \frac{K_2 K_4 K_5}{1 + K_2 K_4 K_5}\left(1 - \frac{p(\mathrm{H_2O})}{P_{\mathrm{eq}}(T)}\right)$
(2I)	$\mathrm{H_2O}_{i,ext} + \mathrm{(s)} \rightleftarrows \mathrm{H_2O{-}(s)}$	$K_2 = \frac{[\mathrm{H_2O{-}(s)}]}{\left[\mathrm{H_2O}_{i,ext}\right][(\mathrm{s})]}$	$v_2 = k_2 K_4 K_5 \left(1 - \frac{p(\mathrm{H_2O})}{P_{\mathrm{eq}}(T)}\right)$
(3I)	$\mathrm{H_2O}_{i,int} \rightleftarrows \mathrm{H_2O}_{i,ext}$	$\left[\mathrm{H_2O}_{i,ext}\right] = \left[\mathrm{H_2O}_{i,int}\right]$	$v_3 = \frac{D_{\mathrm{H_2O}_i}}{l_0} K_4 K_5 \left(1 - \frac{p(\mathrm{H_2O})}{P_{\mathrm{eq}}(T)}\right)$
(4I)	$\mathrm{H_2O_{H_2O}} \rightleftarrows \mathrm{H_2O}_{i,int} + \mathrm{V_{H_2O}}$	$K_4 = \left[\mathrm{H_2O}_{i,int}\right]\left[\mathrm{V_{H_2O}}\right]$	$v_4 = k_4 \left(1 - \frac{p(\mathrm{H_2O})}{P_{\mathrm{eq}}(T)}\right)$
(5I)	$n\left[\mathrm{2Na_{Na}+CO_{3,CO_3}+V_{H_2O}}\right]_h \rightleftarrows n\left[\mathrm{2Na_{Na}+CO_{3,CO_3}}\right]_a$	$K_5 = \frac{1}{\left[\mathrm{V_{H_2O}}\right]^n}$	$v_5 = k_5 \left(\frac{K_1 K_2 K_4}{p(\mathrm{H_2O})}\right)^n \left(1 - \left(\frac{p(\mathrm{H_2O})}{P_{\mathrm{eq}}(T)}\right)^n\right)$

S7. Effect of water vapor on the individual physico-geometrical reaction steps

Table S7. Differential kinetic equations for the IP–SR–PBR(*n*) models with different interface shrinkage dimensions for PBR process

model	Condition	Kinetic equation
IP–SR–PBR(1)	$t - t_{\mathrm{IP}} \leq 1/k_{\mathrm{PBR(1)}}$	$\frac{\mathrm{d}\alpha}{\mathrm{d}t} = k_{\mathrm{PBR(1)}}\left[1 - \exp\left(-k_{\mathrm{SR}}(t - t_{\mathrm{IP}})\right)\right]$
	$t - t_{\mathrm{IP}} \geq 1/k_{\mathrm{PBR(1)}}$	$\frac{\mathrm{d}\alpha}{\mathrm{d}t} = k_{\mathrm{PBR(1)}}\exp\left(-k_{\mathrm{SR}}(t - t_{\mathrm{IP}})\right)\left[\exp\left(\frac{k_{\mathrm{SR}}}{k_{\mathrm{PBR(1)}}}\right) - 1\right]$
IP–SR–PBR(2)	$t - t_{\mathrm{IP}} \leq 1/k_{\mathrm{PBR(2)}}$	$\frac{\mathrm{d}\alpha}{\mathrm{d}t} = -2k_{\mathrm{PBR(2)}}\left[\left(1 + \frac{k_{\mathrm{PBR(2)}}}{k_{\mathrm{SR}}}\right)\exp\left(-k_{\mathrm{SR}}(t - t_{\mathrm{IP}})\right) + k_{\mathrm{PBR(2)}}(t - t_{\mathrm{IP}}) - \left(1 + \frac{k_{\mathrm{PBR(2)}}}{k_{\mathrm{SR}}}\right)\right]$
	$t - t_{\mathrm{IP}} \geq 1/k_{\mathrm{PBR(2)}}$	$\frac{\mathrm{d}\alpha}{\mathrm{d}t} = -2k_{\mathrm{PBR(2)}}\exp\left(-k_{\mathrm{SR}}(t - t_{\mathrm{IP}})\right)\left[1 + \frac{k_{\mathrm{PBR(2)}}}{k_{\mathrm{SR}}} - \frac{k_{\mathrm{PBR(2)}}}{k_{\mathrm{SR}}}\exp\left(\frac{k_{\mathrm{SR}}}{k_{\mathrm{PBR(2)}}}\right)\right]$
IP–SR–PBR(3)	$t - t_{\mathrm{IP}} \leq 1/k_{\mathrm{PBR(3)}}$	$\frac{\mathrm{d}\alpha}{\mathrm{d}t} = -3k_{\mathrm{PBR(3)}}\left[\left(1 + 2\frac{k_{\mathrm{PBR(3)}}}{k_{\mathrm{SR}}} + 2\left(\frac{k_{\mathrm{PBR(3)}}}{k_{\mathrm{SR}}}\right)^2\right)\exp\left(-k_{\mathrm{SR}}(t - t_{\mathrm{IP}})\right) - \left(k_{\mathrm{PBR(3)}}(t - t_{\mathrm{IP}})\right)^2 + 2k_{\mathrm{PBR(3)}}\left(\frac{k_{\mathrm{PBR(3)}}}{k_{\mathrm{SR}}} + 1\right)(t - t_{\mathrm{IP}}) - \left(1 + 2\frac{k_{\mathrm{PBR(3)}}}{k_{\mathrm{SR}}} + 2\left(\frac{k_{\mathrm{PBR(3)}}}{k_{\mathrm{SR}}}\right)^2\right)\right]$
	$t - t_{\mathrm{IP}} \geq 1/k_{\mathrm{PBR(3)}}$	$\frac{\mathrm{d}\alpha}{\mathrm{d}t} = 3k_{\mathrm{PBR(3)}}\exp\left(-k_{\mathrm{SR}}(t - t_{\mathrm{IP}})\right)\left[2\left(\frac{k_{\mathrm{PBR(3)}}}{k_{\mathrm{SR}}}\right)^2\left(\exp\left(\frac{k_{\mathrm{SR}}}{k_{\mathrm{PBR(3)}}}\right) - 1\right) - \left(1 + 2\frac{k_{\mathrm{PBR(3)}}}{k_{\mathrm{SR}}}\right)\right]$

Table S8. Optimized $1/t_{IP}$, k_{SR}, and k_{PBR} values based on the IP–SR–PBR(2) for the thermal dehydration of SC-MH under isothermal conditions in a stream of dry or wet N_2 with different $p(H_2O)_{ATM}$ values

$p(H_2O)_{ATM}$ /kPa	T / K	$(1/t_{IP})$ / s^{-1}	k_{SR} / s^{-1}	$k_{PBR(2)}$ / s^{-1}	$R^{2,\,a}$	
					differential	integral
dry N_2	312.3	3.69×10^{-4}	2.30×10^{-4}	5.59×10^{-5}	0.9906	0.9986
	314.4	4.44×10^{-4}	2.77×10^{-4}	7.28×10^{-5}	0.9871	0.9987
	318.2	9.43×10^{-4}	5.92×10^{-4}	1.14×10^{-4}	0.9964	0.9993
	320.0	2.45×10^{-3}	1.13×10^{-3}	1.67×10^{-4}	0.9986	0.9995
	324.0	3.48×10^{-3}	1.58×10^{-3}	2.48×10^{-4}	0.9960	0.9981
	325.9	4.86×10^{-3}	1.78×10^{-3}	3.36×10^{-4}	0.9984	0.9998
	327.8	1.17×10^{-2}	5.82×10^{-3}	5.34×10^{-4}	0.9959	0.9998
	329.7	-----	5.13×10^{-3}	6.97×10^{-4}	0.9965	0.9997
0.4	323.6	3.30×10^{-4}	2.04×10^{-4}	7.69×10^{-5}	0.9864	0.9999
	325.9	6.10×10^{-4}	3.65×10^{-4}	1.08×10^{-4}	0.9877	0.9990
	328.6	9.65×10^{-4}	6.64×10^{-4}	1.83×10^{-4}	0.9878	0.9987
	330.7	1.50×10^{-3}	1.05×10^{-3}	2.88×10^{-4}	0.9898	0.9980
	332.8	2.26×10^{-3}	1.47×10^{-3}	4.06×10^{-4}	0.9847	0.9981
	334.4	3.65×10^{-3}	2.04×10^{-3}	5.55×10^{-4}	0.9852	0.9980
	336.4	3.75×10^{-3}	2.87×10^{-3}	7.16×10^{-4}	0.9955	0.9977
3.6	339.3	1.82×10^{-4}	1.25×10^{-4}	6.19×10^{-5}	0.9697	0.9992
	340.8	2.50×10^{-4}	2.16×10^{-4}	1.15×10^{-4}	0.9834	0.9998
	343.9	6.67×10^{-4}	5.86×10^{-4}	2.69×10^{-4}	0.9877	0.9997
	346.0	1.11×10^{-3}	1.01×10^{-3}	4.26×10^{-4}	0.9869	0.9997
	348.2	1.40×10^{-3}	1.57×10^{-3}	7.52×10^{-4}	0.9982	0.9995
8.9	352.0	1.22×10^{-4}	2.08×10^{-4}	9.30×10^{-5}	0.9516	0.9999
	353.8	3.50×10^{-4}	4.34×10^{-4}	1.69×10^{-4}	0.9716	0.9992
	355.4	8.19×10^{-4}	8.31×10^{-4}	3.06×10^{-4}	0.9670	0.9989
	356.8	1.05×10^{-3}	1.25×10^{-3}	5.33×10^{-4}	0.9900	0.9994
	359.5	2.50×10^{-3}	2.50×10^{-3}	9.22×10^{-4}	0.9845	0.9993
	362.0	4.00×10^{-3}	4.44×10^{-3}	1.57×10^{-3}	0.9929	0.9993

[a] Determination coefficient of the nonlinear least-squares analysis.

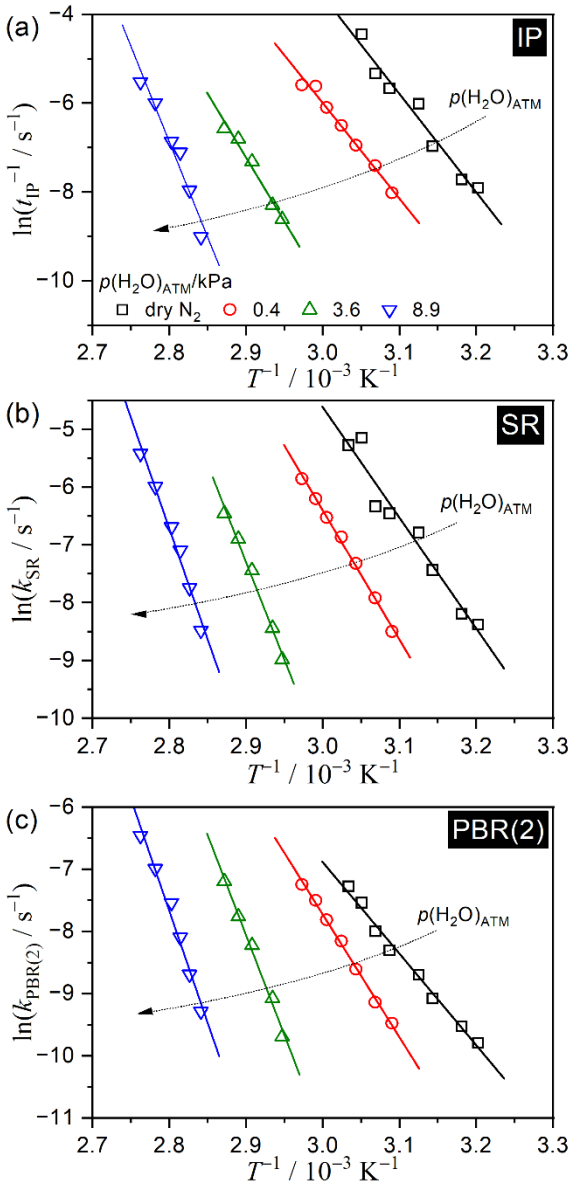

Figure S14. Conventional Arrhenius plots for the component physico-geometrical reaction steps of the thermal dehydration of SC-MH under isothermal conditions in a stream of dry or wet N_2 with different $p(H_2O)_{ATM}$ values, examined according to eq. (19): (a) IP, (b) SR, and (c) PBR(2).

Table S9. Apparent kinetic parameters for the IP, SR, and PBR(2) processes of the thermal dehydration of SC-MH under isothermal conditions in a stream of dry or wet N_2 with different $p(H_2O)_{ATM}$ values, examined according to eq. (19)

Process	$p(H_2O)_{ATM}$ / kPa	E_a / kJ mol^{-1}	ln(A / s^{-1})	$-\gamma$ [a]
IP	dry N_2	183.7 ± 15.7	62.7 ± 5.9	0.9824
	0.4	179.1 ± 9.9	58.6 ± 3.6	0.9924
	3.6	239.2 ± 20.1	76.2 ± 7.1	0.9896
	8.9	357.1 ± 39.3	113.4 ± 13.3	0.9766
SR	dry N_2	159.2 ± 14.2	52.8 ± 5.3	0.9770
	0.4	186.2 ± 4.9	60.8 ± 1.8	0.9983
	3.6	281.2 ± 15.4	90.8 ± 5.4	0.9955
	8.9	318.8 ± 20.4	100.7 ± 6.9	0.9919
PBR(2)	dry N_2	122.4 ± 5.3	37.3 ± 2.0	0.9944
	0.4	164.3 ± 4.3	51.6 ± 1.6	0.9983
	3.6	267.3 ± 13.9	85.2 ± 4.9	0.9959
	8.9	299.6 ± 20.8	93.2 ± 7.0	0.9905

[a] Correlation coefficient of the linear regression analysis.

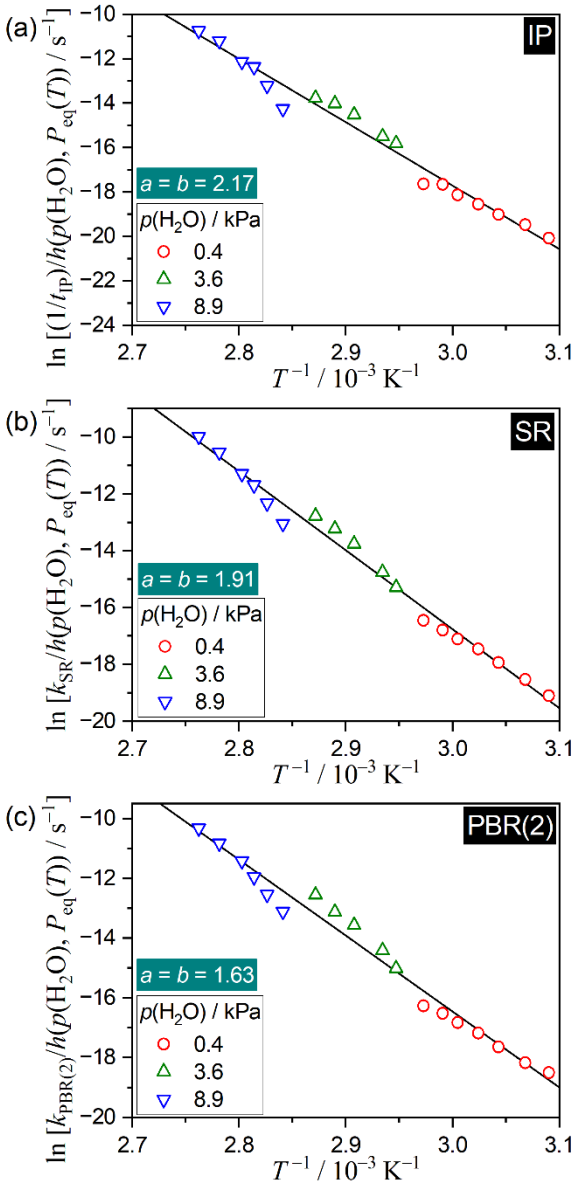

Figure S15. Extended Arrhenius plots for the component physico-geometrical reaction steps of the thermal dehydration of SC-MH under isothermal conditions in a stream of wet N_2 with different $p(H_2O)_{ATM}$ values, examined according to eq. (20) and AF in eq. (10) with the restriction of $a = b$: (a) IP, (b) SR, and (c) PBR(2).